Article

Study on Instability Characteristics of the Directional Borehole on the Coal-Seam Roof: A Case Study of the Tingnan Coal Mine

Zhie Wang [1] **, Xin Yang** [2,3,4,*] **, Gongda Wang** [3,4,*] **and Haiwen Gong** [5]

1 School of Management Engineering, Capital University of Economics and Business Beijing, Beijing 100083, China; 12021210006@cueb.edu.cn
2 Research Institute of Macro-Safety Science, University of Science and Technology Beijing, Beijing 100083, China
3 School of Civil and Resources Engineering, University of Science and Technology Beijing, Beijing 100083, China
4 State Key Laboratory of the Ministry of Education of China for High-Efficient Mining and Safety of Metal Mines, University of Science and Technology Beijing, Beijing 100083, China
5 School of Emergency Management and Safety Engineering, China University of Mining and Technology (Beijing), Beijing 100083, China; sqt191010116@student.cumtb.edu.cn
* Correspondence: b2081146@ustb.edu.cn (X.Y.); b1936282@ustb.edu.cn (G.W.)

Abstract: Directional long drilling on the roof is an effective gas control measure in the goaf, but there is little research on the stability of the surrounding rock. In this study, the geological conditions of the #4 coal seam in the Tingnan Coal Mine, Shaanxi Province, China taken as the application background, and the deformation characteristics of boreholes under four typical coal and rock conditions were first analyzed based on the Universal Distinct Element Code (UDEC) numerical simulation. Secondly, the stress, strain, and plastic deformation of the rock surrounding the borehole with different diameters were carried out using the Fast Lagrangian Analysis of Continua 3D (FLAC 3D). The effect of the casing on the stability of the borehole was also simulated. The results showed that the borehole stability of coal and mudstone was lower than that of fine-grained sandstone and coarse-grained sandstone. The larger the borehole diameter, the lower the stability. The borehole tended to be unstable, especially when the diameter was 160 mm and 200 mm. Traditional pipes can provide some protection, but for large boreholes, the protection is poor. Based on the above research, uniaxial compression tests were carried out on various internal support tubes, such as 'line-shaped', 'Y-shaped', and 'cross-shaped'. The results showed that the cross-shaped pipe had the highest compressive strength, which was 4–5 times that of the other types of protective pipe and had a good protective effect. The research results can provide reliable technical support for the protection of directional boreholes on roofs through strata and have important implications for the popularization and application of the directional long borehole technique.

Keywords: directional long borehole on the roof; borehole stability; lithology; borehole diameter; internal support borehole protection pipe

1. Introduction

The gas disaster is one of the major disasters that threaten coal mine safety production. With the development of coal resources gradually extending to the depths, the difficulty of gas control is increasing. Borehole drainage is the basic gas control measure. At present, gas pre-drainage mainly includes the borehole drilling in the bedding coal seam and the penetrating borehole in the bottom roadway, which can penetrate the coal seam so that the gas easily flows into the boreholes along the bedding plane, which can effectively reduce the gas content in the coal seam [1–4]. Buried pipe drainage, high-level drilling, and roof directional drilling are mainly used for gas control in the goaf during mining. Because the roof directional borehole is located in the fracture zone of the coal seam, where the horizon

is high and less affected by mining disturbance, the borehole and gas drainage life cycle is long, which can effectively solve the problem of gas overflow in the upper corner of the goaf [5–8].

However, the openings of roof directional boreholes are often located in the coal seam, and they have to pass through mudstone and sandstone before entering the fracture zone. Due to the large diameter of the borehole (typically around 160 mm), the boreholes are susceptible to loss of stability resulting in deformation and collapse. Therefore, the stability of the directional borehole on the roof through the strata directly affects its drainage effect. Borehole diameter, lithology, and other parameters are important parameters affecting borehole stability [9,10].

Research on the influencing factors of borehole stability and borehole failure modes in the bedded coal seam has been conducted by scholars at home and abroad. The influencing factors of borehole stability mainly include rock strength, gas pressure, stress and strain, burial depth, lateral pressure coefficient, and anisotropic permeability [11–14]. Yang et al. [15] indicated that rock mechanics is the main theoretical basis for ensuring good stability, sand production, or casing damage. Karatela et al. [12] investigated the stability of boreholes in fractured rock using the discrete element method. The results show that the stability of boreholes depends largely on the strength of the rock. The tensile and shear failure of the borehole increases with increasing fluid velocity and pore pressure. Ding et al. [16] found that the large difference in permeability of rock layers around the borehole would lead to the change in stress state, damage area, collapse pressure, and fracture pressure around the borehole. Zhao et al. [17] studied the instability characteristics of the borehole under steady vertical load using the gas drainage borehole collapse dynamic monitoring devices. The attenuation of the borehole circumferential strain is an important symbol for the prediction and warning of borehole instability and collapse. A borehole may be damaged resulting from the integrated effect of stratigraphic and structural factors. Katanov et al. [18] proposed a model based on neural simulation to analyze the deformation of rock layers with different strength characteristics. Ma et al. [19] solved the problem of severe borehole deviation in coal mine gas drainage by summarizing the borehole deviation law and improving the precision directional drilling tool. Dychkovsky et al. [20] simulated the influence of geological faults on the stress and deformation state of rock mass by FLAC 5.00 and established a three-dimensional network visualization by computer simulation results and data interpolation method. The research shows that in the Lviv-Volyn coal basin, the geological fault of up to 3 m distance has a great influence on the stress and deformation state of the rock mass. Based on the parameters of the geo-mechanical model developed and confirmed, Petlovanyil et al. [21] have determined the reasonable range of inclination angle and key parameters of the radius of curvature when using underground gasification technology to develop thin coal seams. Zhang et al. [22] numerically simulated the deformation characteristics of boreholes with different burial depths, and the results showed that the deeper the burial depth, the more obvious the deformation. The form of instability and failure was the collapse of the upper part, and the fracture of the left and right sides formed the fracture area. Qu et al. [23] found that the stability of coal seam borehole was affected by the time lag effect based on field tests and numerical simulation; they found that the change of pore pressure was the main factor affecting the time lag effect, and the rich cleat was the internal factor. Niu et al. [24,25] studied the monitoring and evaluation of borehole stability through experiments and simulations, proposed an index to calculate the degree of borehole damage based on the residual area, and fitted the functional equation between the relative pressure of the sensor (the difference between the real-time pressure of the sensor and the coupling pressure of the borehole wall) and the degree of borehole damage. Combined with the amount of gas extracted, it was verified that the borehole deformation first increased and then became stable with time, and then increased and then decreased with depth. Zhang et al. [26] established the gas migration channel zoning model and determined the parameters of the optimal directional long borehole in the working face by using UDEC and COMSOL software. Xu et al. [27] found that when

the borehole is shallow, the friction resistance between the drill pipe and the borehole wall increases linearly. With the increase of borehole depth, the friction resistance gradually develops into an exponential relationship. In addition, Liu et al. [28] concluded that the effective drainage radius of a directional long drilling hole has an exponential relationship with the distance from the drilling opening. Yuan et al. [29,30] conducted the combined drilling method of curtain grouting in underground deep wells, which can significantly reduce the risk of water inrush in deep mining with complex hydrogeological conditions. A mathematical model to describe the unstable pressure dynamics in stress-sensitive coalbed methane reservoirs was proposed by Wang et al. [31]. Wang et al. [32] proposed the gradient recognition and memory-cutting method for the continuous advancement of non-uniform coal seams, such as coal seams with folded structures on long-arm working-face.

Moreover, scholars have conducted a great number of field tests and research on a series of borehole protection technologies, such as borehole reinforcement, regional solidification, and screen protection. Xue et al. [33] found that increasing the casing strength and thickness can effectively control the borehole instability and greatly improve the gas extraction effect through field tests. To improve the stability of the borehole. Zhai et al. [34] conducted research on the technology of screen pipe protection. By comparing the maximum AE event technology and energy dissipation rate, it was found that the screen pipe can effectively resist external stress disturbance, prevent hole collapse, and improve the drainage effect of the borehole. Di et al. [35] proposed the regional solidification pore formation method for soft coal seams, which can solidify the strength of the rock surrounding the borehole and improve the pore formation rate. Qi et al. [36] tested the full-hole deep screen mesh tube drainage technology to solve the problem of internal collapse and negative pressure loss of deep coal seam drainage boreholes, which can effectively control the collapse and deformation of boreholes and reduce the negative pressure loss. Compared with conventional drainage, after 90 days, the gas drainage concentration increased by 101% and the gas flow increased by 97%, so the gas drainage rate increased significantly. Li et al. [37] proposed to integrate the technology of borehole digging, protection, and sealing in the construction of the borehole site, so as to strengthen the stability of the borehole and solve the problems of difficult borehole formation, poor drainage effect and high danger of coal seam explosion in soft coal seams.

Currently, the research on borehole stability mainly focuses on the surrounding rock stress, burial depth, lateral pressure coefficient, anisotropic permeability, and other influencing factors, and the failure characteristics of the borehole in the bedding coal seam, while the research on the stability and borehole protection technology of roof directional long borehole is still lacking. Compared with the traditional high-position alley gas extraction technology, the roof directional long borehole has the advantages of a short construction period, low investment, and long extraction period. Therefore, the stability of the roof-directional long borehole with different lithology and borehole diameters was analyzed by numerical simulation in this paper. The compression experiments were carried out to study the protective effect of different internal support structures in the directional borehole, which is beneficial to realize the effective hole formation of the directional long borehole on the roof and high-efficiency gas extraction in the goaf treatment of the coal mine face. This paper will provide some guidance for the popularization and application of directional long boreholes on the roof technology, and also gradually realize the "replacing alley with borehole" in goaf gas treatment. The rest of this study is organized as follows. Section 2 analyzes the deformation characteristics of boreholes under different coal and rock conditions, and simulates the stress, strain, and plastic deformation of rocks around boreholes with different diameters. In Section 3, the experiment on the influence of the internal support hole protection tube on the stability of the hole wall was carried out. Section 4 analyzes the mechanism of numerical simulation and laboratory experiment results. Finally, the conclusions are presented in Section 5.

2. Numerical Simulation of the Borehole Stability

Lithology, borehole diameter, and borehole protection tubing have a great influence on the stability of the borehole; for example, the strength of the rock will affect the rate of hole formation and the durability of the borehole. The larger the diameter of the borehole, the closer it is to the uniaxial compressive strength of the rock and the easier it is to destroy the stability of the borehole in the rock formation. The shear strength of the casing is also closely related to the effectiveness of the casing [38–40]. Therefore, this section takes the 208-working face of Tingnan Coal Mine in Xianyang, Shaanxi Province, China as an object to conduct numerical simulation research to analyze the influence of lithology, borehole diameter, borehole protection pipe, and other factors on borehole stability. Tingnan Mine Field is mainly covered by Quaternary loess and Tertiary red soil, and the Lower Cretaceous Luohe Formation is exposed in major valleys along the Heihe River and Jinghe River. The strata in the minefield of Tingnan Coal Mine are, from top to bottom, Holocene (Q_4), Upper Pleistocene Malan Formation (Q_3), Quaternary-Middle Pleistocene Lishi Formation (Q_2), Huachi Formation (K_{1h}), Luohe Formation (K_{1l}), Lower Cretaceous Yijun Formation (K_{1y}), Anding Formation (J_{2a}), Zhiluo Formation (J_{2z}) and Middle Cretaceous Yanan Formation. The Jurassic Yan'an Formation is a coal-bearing layer, and the Triassic Hujiahe Formation is a direct or indirect sedimentary basement. The surface and overlying strata are basically the same, and the aquifer of the Luohe Formation is in the upper part. The minefield is located in the middle part of the anticline (Lujia–Xiaolingtai), and the stratum in the middle is close to the level. The terrain in the south wing is gentler than that in the north wing, and the dip angle in the north wing is 4°~6°. The back of the syncline is Mengcun, which is connected with the north wing of the anticline from Lujia to Xiaolingtai. The strike of the layer is N 20° E and the dip angle is about 2°. The north wing crosses the Great Buddha Temple to the south and the occurrence of the southeast corner of the layer changes. The anticline structure affects the change of layer thickness, coal seam thickness, and occurrence in the minefield. Tingnan coal mine is a high-gas mine, and the 4# coal seams belong to the type II spontaneous combustion coal seams, and the coal dust is explosive. The coal seam thickness of the 208-working face varies greatly, with the average coal seam thickness being 11.5 sm. The base roof of the working face is coarse-grained sandstone, which is grey and mainly composed of quartz and feldspar. The immediate roof is mudstone, dark grey and lumpy, containing a large number of plant fossils and locally a small number of calcite veins. The direct floor is aluminum mudstone, light grey, dense, and contains plant root fossils. The base is fine-grained sandstone, light grey, chestnut, and hard, with sandy muddy breccias. The 208-working face is located in the west wing of the second panel, with a total length of 2527 m. The description of formation lithology characteristics is shown in Table 1.

Table 1. The description of formation lithology in 208 working-face.

| Stratigraphic Category	Rock Category	Average Thickness	Characteristics of the Lithology
Basic roof	Coarse-grained sandstone	$\dfrac{11.63\sim49.24}{30.5}$	Coarse-grained sandstone, gray, mainly composed of quartz and feldspar, sub-round, argillaceous cementation, wavy bedding, mixed with thin siltstone, locally containing siderite nodules, which is obviously in contact with the underlying.
Direct roof	Mudstone	$\dfrac{1.3\sim5.06}{2.07}$	Mudstone, gray, dark gray, lumpy, containing a large number of plant fossils, locally containing a small number of calcite veins, with a slip surface on the upper part and obvious contact with the underlying.
Direct floor	Aluminous mudstone	$\dfrac{0.94\sim3.2}{1.98}$	Aluminous mudstone, light gray, dense, containing plant root fossils, with a sliding surface at the broken part.
Basic floor	Fine-grained sandstone	$\dfrac{2.8\sim19.8}{9.51}$	Fine-grained sandstone, light gray, reddish brown, relatively hard, containing sandy argillaceous breccia.

2.1. Analysis of the Influence of Lithology on the Borehole Stability

2.1.1. Model Building

Given that the roof-directed long borehole has a large span in the roof, the horizon and rock lithology through which the hole passes is complex. The borehole stability of coal, mudstone, fine-grained sandstone, and coarse-grained sandstone in the working face rock mass was investigated using the Universal Distinct Element Code (UDEC). The model is 300 m long and 180 m high as shown in Figure 1a. According to the histogram distribution of rock layers, joints are set and grids are divided, and the number of grids is 2,976,224. At the upper boundary of the model, the self-weight stress of the overlying strata is imposed, and the simulated mining depth is 430 m. According to the actual situation, it is assumed that the left and right sides are mined together, and the distance between the mining boundary and the left and right boundaries of the model is 60 m, each mining is 10 m, and the mining length is 180 m. To facilitate simulation and calculation, the model is partially simplified: The change in coal seam dip angle and thickness is ignored, and the calculation is based on the average coal seam thickness. Considering the large span of high-level directional drilling in horizontal and vertical directions, the strata and rock lithology through which the drilling passes are also complicated. Therefore, these study models and analyzes the stability of high-level directional drilling under different lithologies based on mining disturbance. Considering the different lithologic horizons that are encountered in drilling practice, four main rock layers are selected for study in the model, namely coal rock, mudstone, fine-grained sandstone, and coarse-grained sandstone. Given that the roof-directed long borehole has a large span in the roof, the horizon and rock lithology through which the hole passes is complex. The borehole stability of coal, mudstone, fine-grained sandstone, and coarse-grained sandstone in the working face rock mass was investigated using the UDEC. A 1 m × 1 m rock mass model with a 130 mm aperture is created as shown in Figure 1b,c. In this model, Voronoi is used to generate joints, and the blocks are distributed in triangular mesh elements. The upper boundary is set as the vertical downward self-weight stress boundary, the lower boundary is fixed as a constraint, and the left and right boundaries are restricted horizontal displacements, as shown in Figure 2. When the calculation model is set, the model should be assigned according to the constitutive model. The Coulomb slip model is selected for numerical simulation, and the rock mechanics parameters of 208 working faces in the Tingnan Coal Mine are shown in Table 2.

**Table 2.** The rock mechanics parameters.

Lithology	Bulk Modulus/(GPa)	Shear Modulus/(GPa)	Cohesive Strength/(MPa)	Internal Friction/(°)	Density/(kg/m^3)	Tensile strength/MPa	Source
Coal	1.42	0.57	1.2	28	1400	0.64	Lab measurement
Mudstone	4.54	4.31	2.08	32	2560	1.32	Lab measurement
Coarse-grained sandstone	4.58	4.42	2.57	34	2530	1.28	Lab measurement
Fine-grained sandstone	4.64	4.32	4.57	35	2540	1.35	Lab measurement
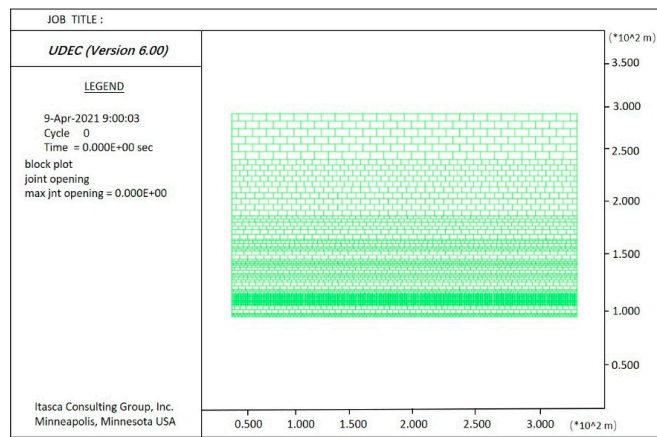
(**a**) Coal seam mining model of directional drilling structure
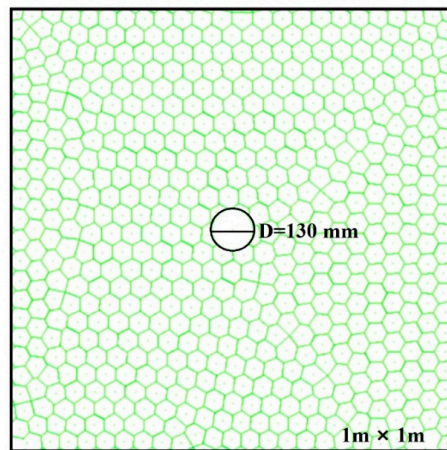
(**b**) Joint distribution
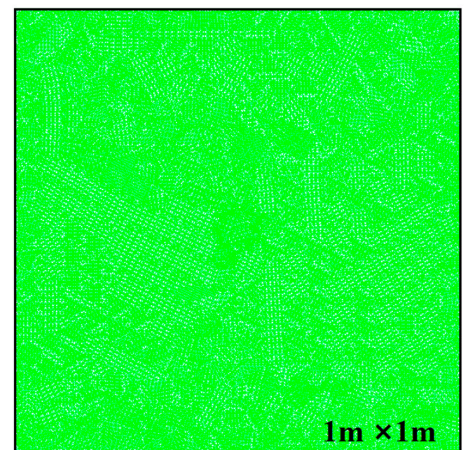
(**c**) Grid division

Figure 1. The Numerical computation models. (**a**) The model of the coal seam mining model of directional drilling structure; (**b**) the joint distribution of the model; (**c**) the grid division of the model.
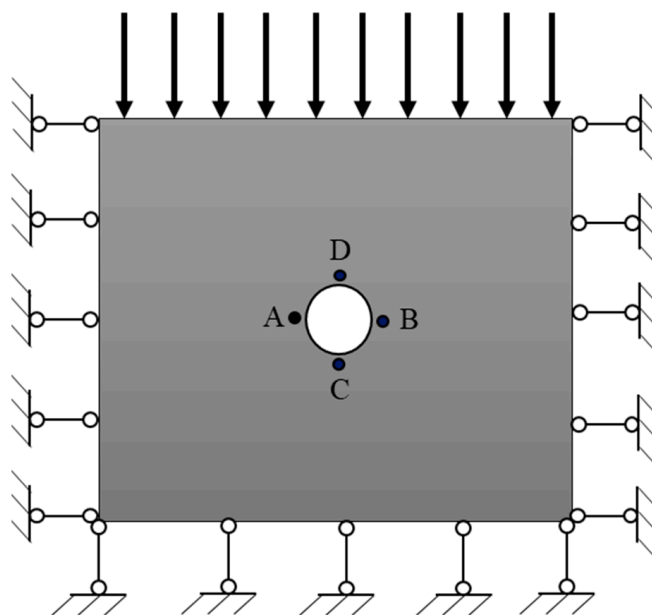

Figure 2. Schematic diagram of boundary constraints.

2.1.2. Analysis of the Simulation Results

(1)   Variation of the Borehole Stress

The stress variation range of the surrounding rock is shown in Figure 3. The stress around the borehole in coal and rock ranges from 1.92 MPa to 35.57 MPa, that which around the borehole in mudstone ranges from 1.77 MPa to 29.84 MPa, that which around the borehole in fine-grained sandstone ranges from 1.49 MPa to 27.58 MPa, and that which is around the borehole in coarse-grained sandstone ranges from 1.71 MPa to 27.20 MPa. From the stress range, it can be seen that coal and mudstone have large stress peaks and stress fluctuations, while the stress ranges of fine-grained sandstone and coarse-grained sandstone are relatively small and proximate to each other.
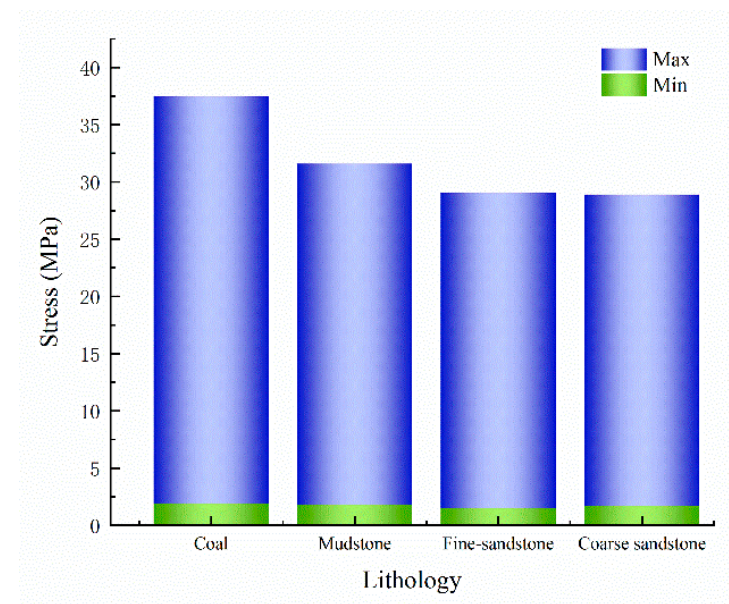

Figure 3. Stress range under different lithologies.

The maximum principal stress contour of the borehole is shown in Figure 4. The peak value of the maximum principal stress is mainly distributed in some borehole walls near the left and right sides of the borehole, while the rest of the rock mass is evenly distributed with lower stress. The maximum principal stress results of different lithologies show that the stress concentration of coal and mudstone is higher, the high-stress area of rock mass around the borehole is larger, and the stress distribution of fine-grained sandstone and coarse-grained sandstone is relatively more uniform. It indicates that the stress state of coal and mudstone is unstable.

(2)   Variation of the borehole displacement

The displacement contour of the boreholes with different lithologies is shown in Figure 5. As can be seen from Figure 5, the overall displacement trend of the borehole under the four lithologies is similar, and the displacement is all in the direction of the borehole center. The displacement of the rock mass around the borehole is small, and the displacement of the rock mass on the upper and lower sides of the borehole is larger than that on the left and right sides. However, there are still some differences in the borehole displacement of different lithologies. The borehole displacement of coal and mudstone is obviously larger than that of fine-grained sandstone and coarse-grained sandstone, especially on the upper and lower sides of the borehole. The block with the largest displacement is coal, followed by mudstone. The four lithologies are similar on the left and right sides.
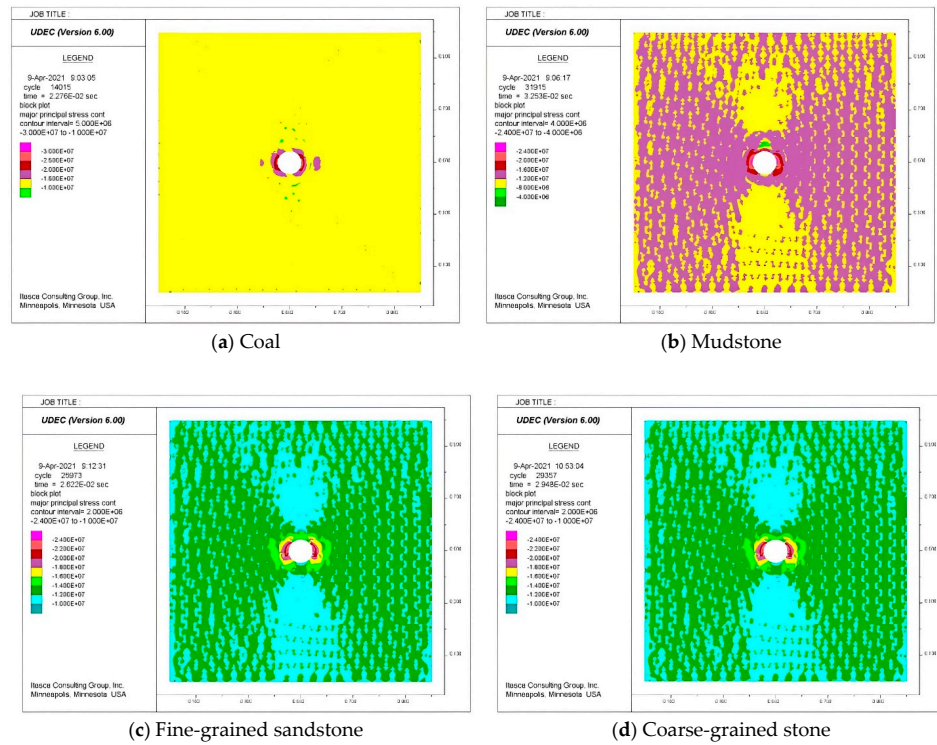
(**a**) Coal

(**b**) Mudstone

(**c**) Fine-grained sandstone

(**d**) Coarse-grained stone

Figure 4. Maximum principal stress contours. (**a**) The maximum principal stress contour of the coal; (**b**) the maximum principal stress contour of the mudstone; (**c**) the maximum principal stress contour of the fine-grained sandstone; (**d**) the maximum principal stress contour of the coarse-grained sandstone.
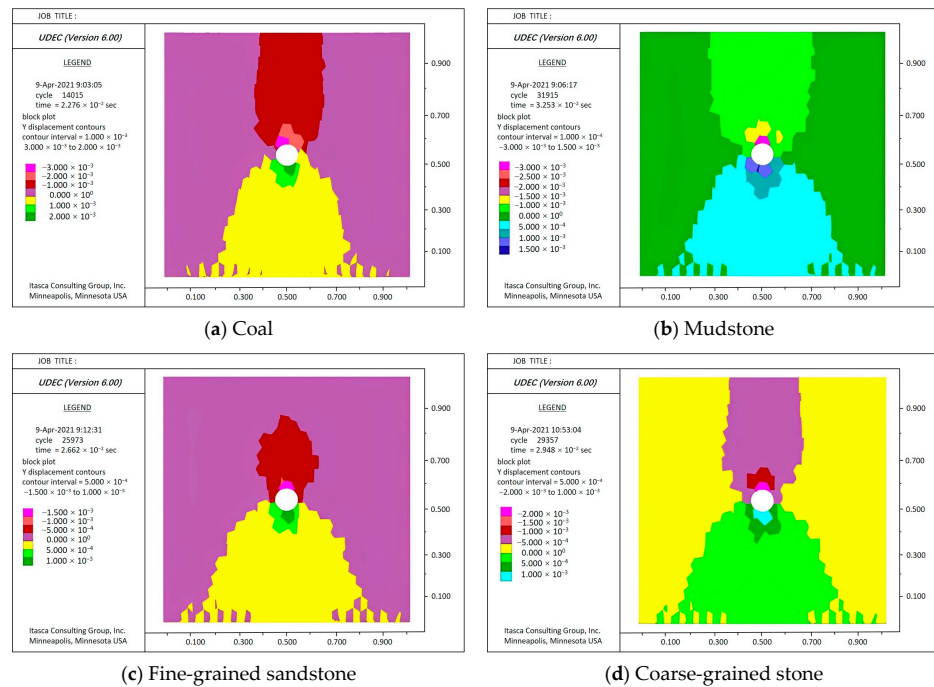

(**a**) Coal

(**b**) Mudstone

(**c**) Fine-grained sandstone

(**d**) Coarse-grained stone

Figure 5. Displacement cloud map in Y direction. (**a**) The displacement cloud map in Y direction of the coal; (**b**) the displacement cloud map in Y direction of the mudstone; (**c**) the displacement cloud map in Y direction of the fine-grained sandstone; (**d**) the displacement cloud map in Y direction of the coarse-grained sandstone.

During the simulation, four measuring points A, B, C, and D were set at the top, bottom, left, and right sides of the borehole. The displacement change of the measuring point is shown in Figure 6. The displacement of each monitoring point first increases and then tends to be stable within the hole. The maximum displacement of the four points is 3.15 mm of the coal at point D, and the minimum is 0.49 mm of the fine-grained sandstone at point A, which shows that the rock mass around the borehole of each lithology is only slightly displaced and remains unchanged. The results of the four measuring points show that the displacement of the coal rock is significantly larger than that of the other three lithologies, and the displacement of the mudstone is also larger than that of the other two lithologies. The displacement changes of fine-grained sandstone and coarse-grained sandstone are similar, and that of coarse-grained sandstone is slightly larger than that of fine-grained sandstone. The results show that there are differences in rock mass displacement around the borehole under different lithologies, which are caused by different rock mechanical parameters. The density, bulk modulus, shear modulus, and tensile strength of coal and mudstone are all low, which leads to cracking or even fracturing of the surrounding rock mass after the borehole is drilled, and then the displacement changes.
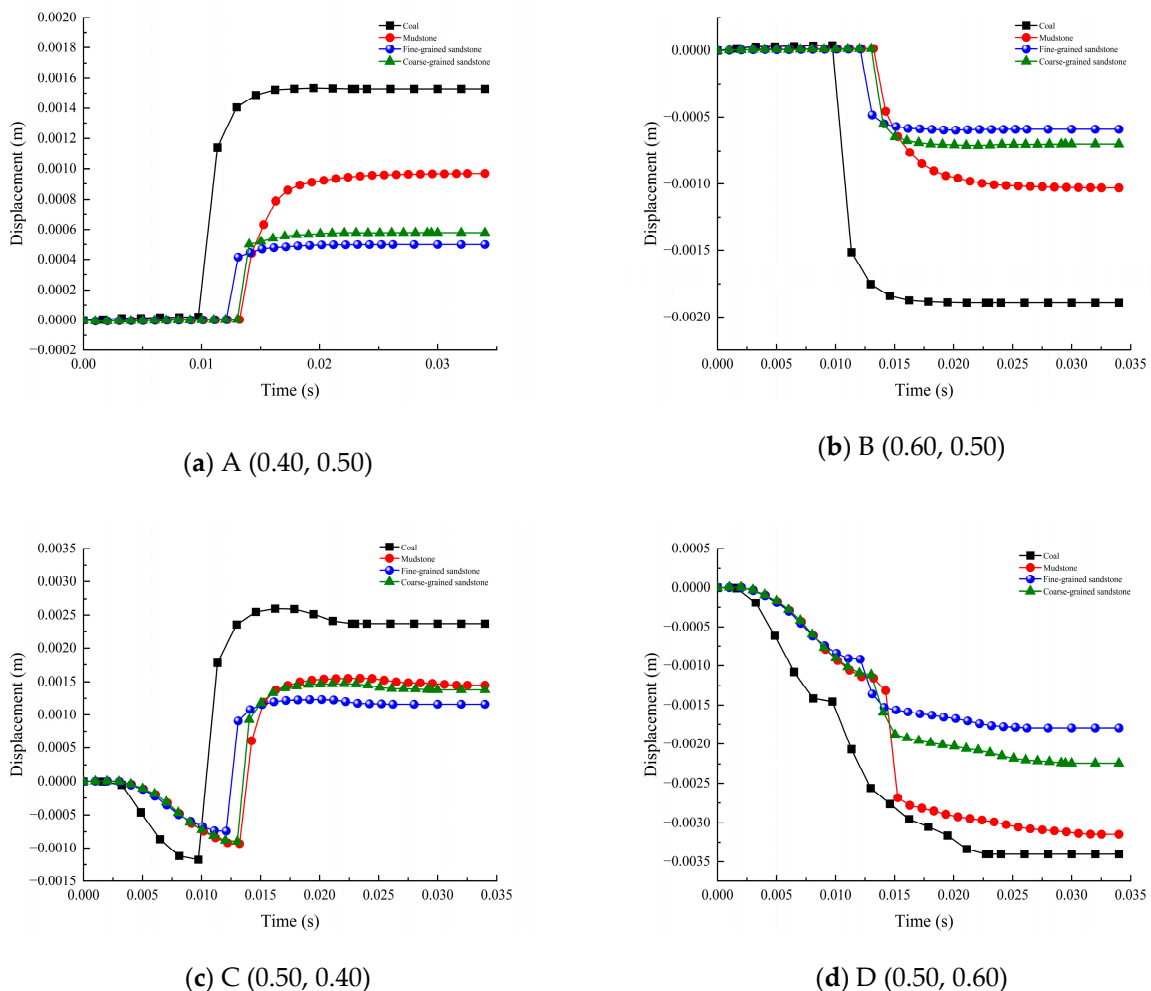

(**a**) A (0.40, 0.50)

(**b**) B (0.60, 0.50)

(**c**) C (0.50, 0.40)

(**d**) D (0.50, 0.60)

Figure 6. Displacement variation under different lithologies. (**a**) The displacement variation in the A (0.40, 0.50); (**b**) the displacement variation in the A (0.60, 0.50); (**c**) the displacement variation in the A (0.50, 0.40); (**d**) the displacement variation in the D (0.50, 0.60).

In summary, the stress and displacement changes of the rock mass around the borehole are obviously larger in the coal and mudstone than in the fine-grained sandstone and coarse-grained sandstone, and the stress and displacement of the rock mass after the borehole is

drilled are strongly influenced by the lithology, which also shows that the borehole stability is high in the fine-grained sandstone and coarse-grained sandstone, while that in the coal and mudstone is poor.

2.2. Analysis of the Influence of Borehole Diameter on Borehole Stability

A three-dimensional borehole model is created based on FLAC 3D and the borehole stability of four diameters, namely 100 mm, 130 mm, 160 mm, and 200 mm, is investigated. The borehole model is shown in Figure 7. The Moore-Coulomb constitutive model is selected for the simulation, which is suitable for solving rock mechanics and excavation problems. The initial stress is $S_{xx} = -1.1985 \times 10^7$ Pa, $S_{yy} = -1.1985 \times 10^7$ Pa, $S_{zz} = -1.1985 \times 10^7$ Pa, and the lateral pressure coefficient is 1.0. The velocity of the left and right boundaries in the X direction is set to 0; the velocity of the bottom boundary in the Y direction is set to 0; and the top boundary is set to the gravity of the overlying strata. Then the excavation simulation was started after reaching the equilibrium level.
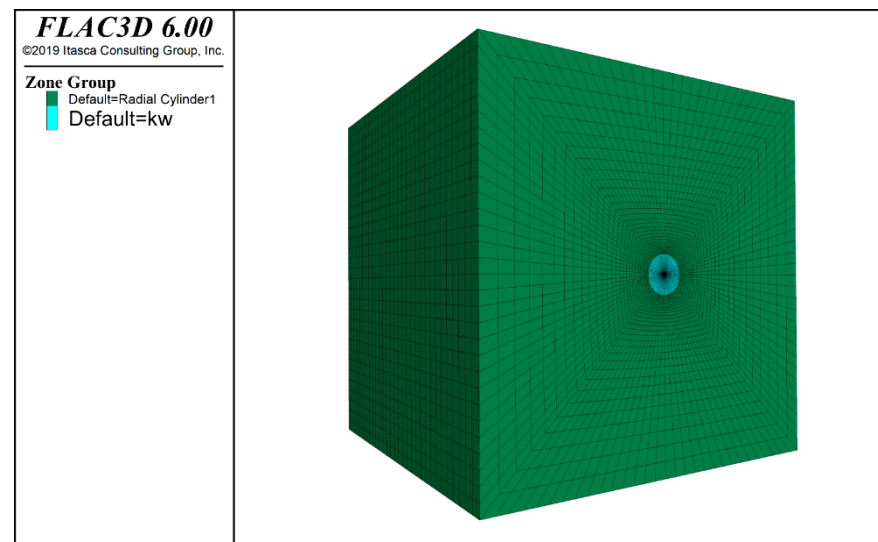

Figure 7. The borehole model.

2.2.1. Analysis of the Stress and Displacement

The maximum principal stress contour of boreholes of different diameters is shown in Figure 8. The maximum principal stress nephogram at 100 mm and 130 mm is distributed in a regular and uniform circle around the borehole, and it begins to deform into an ellipse at 160 mm, while the contour is completely deformed at 200 mm, and the stress expands to the boundary region, resulting in stress equilibrium and instability of the surrounding rock. Thus, the results indicate that when the borehole diameter exceeds 160 mm, the maximum principal stress distribution of the borehole begins to deform, the stress balance tends to be destroyed, and the stress concentration area is proportional to the borehole diameter.

The displacement monitoring of the rock mass around the borehole is shown in Figure 9. According to the curve, the displacement range of the left side of the borehole is 0~3.5 mm, and the displacement ranges of the upper and lower sides are 0~12 mm and 0~25 mm, respectively. The displacement of the left side of the borehole is the smallest, and the displacement of the upper and lower sides of the borehole is much larger than that of the left side, indicating that the borehole damage is mainly caused by the large deformation of the upper and lower sides. The displacement of each monitoring point increases with the hole diameter, and the displacement of the rock mass around the hole changes more. Boreholes with different diameters produce displacements at almost the same time after drilling and then gradually stabilize.
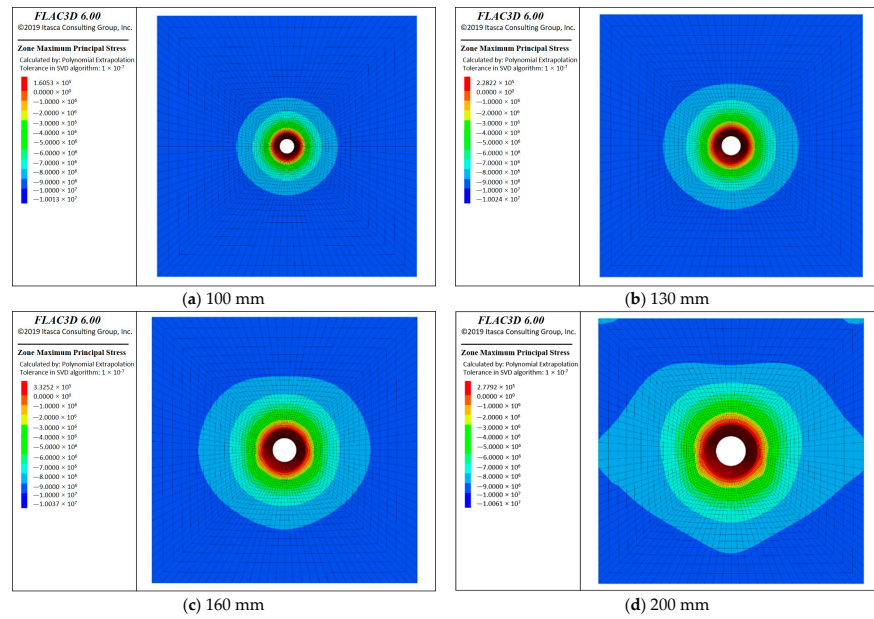
(**a**) 100 mm   (**b**) 130 mm

(**c**) 160 mm   (**d**) 200 mm

Figure 8. Maximum principal stress contours. (**a**) The maximum principal stress contour of the borehole of diameter of 100 mm; (**b**) the maximum principal stress contour of the borehole of diameter of 130 mm; (**c**) the maximum principal stress contour of the borehole of diameter of 160 mm; (**d**) the maximum principal stress contour of the borehole of diameter of 200 mm.
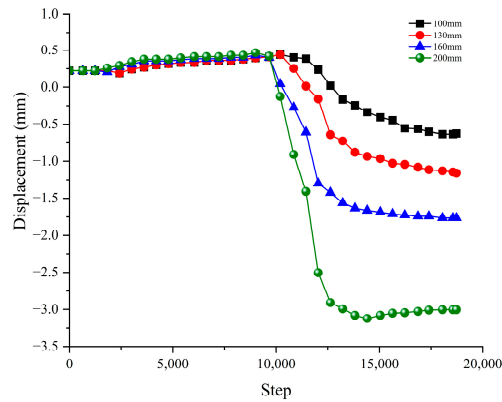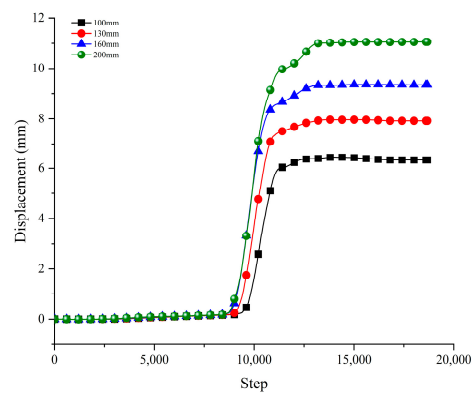

(**a**) Borehole left surrounding rock
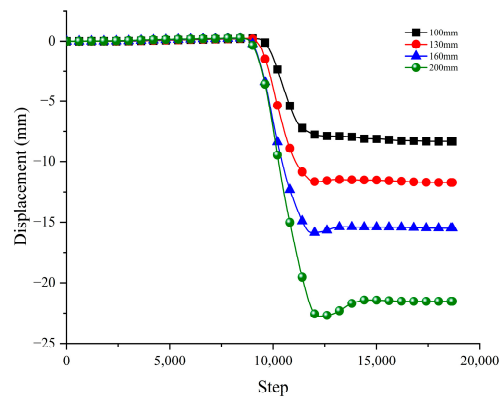
(**b**) Borehole upper surrounding rock

Figure 9. *Cont.*

(**c**) Borehole under a surrounding rock

Figure 9. The variation curve of surrounding rock displacement with different diameters. (**a**) The variation curve of borehole left rock displacement with different diameters; (**b**) the variation curve of borehole upper rock displacement with different diameters; (**c**) the variation curve of borehole under rock displacement with different diameters.

2.2.2. Analysis of the Plastic Failure

The S-distribution and volume of plastic failure of the surrounding rock mass of boreholes are shown in Figures 10 and 11. The distribution of plastic failure zones is similar to that of the vertical stress and is symmetrical, extending around the hole wall. The volumes of plastic failure zones with four diameters of 100 mm, 130 mm, 160 mm, and 200 mm are 0.007 m^3, 0.012 m^3, 0.018 m^3, and 0.03 m^3 respectively. As the borehole diameter increases, so does the extent and volume of the plastic failure zone. The volume of the plastic failure zone can be divided into shear failure and tensile failure. The volume of tensile failure changes very little with the increase in pore diameter as can be seen from Figure 11. On the contrary, the volume of shear failure increases linearly with the increase in pore diameter and is much larger than that of tensile failure in all four-borehole diameters. Therefore, it can be concluded that the failure mode of the boreholes is mainly shear failure.
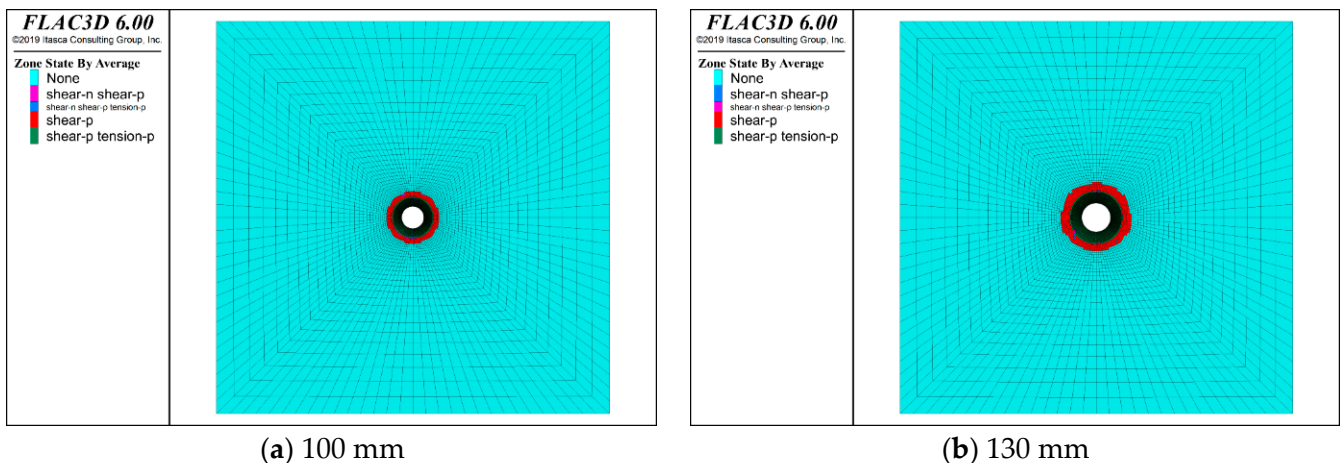

(**a**) 100 mm

(**b**) 130 mm

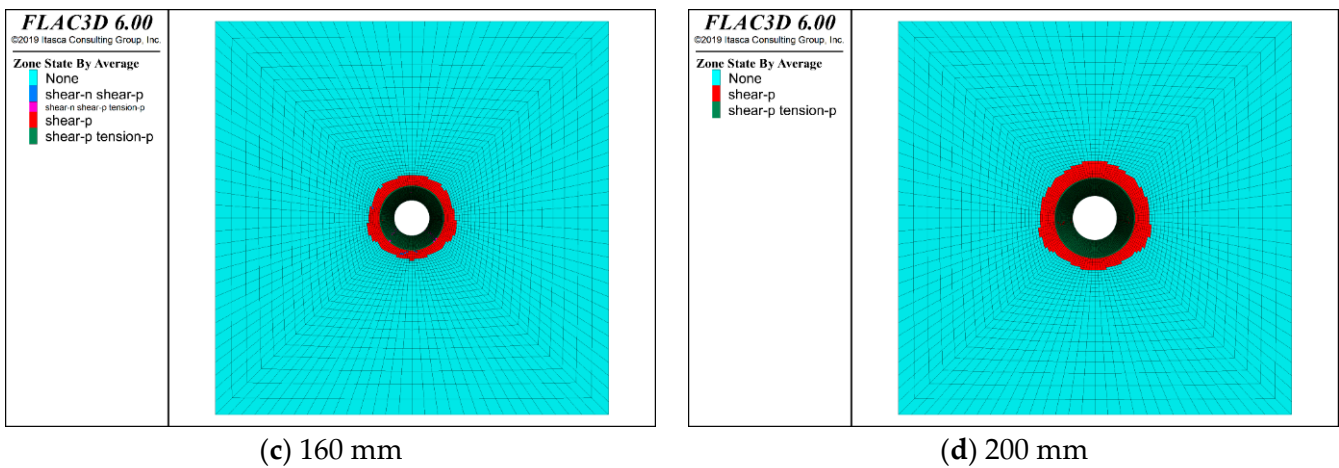**Figure 10.** *Cont.*

(**c**) 160 mm

(**d**) 200 mm

Figure 10. Distribution of plastic failure of boreholes with different diameters. (**a**) The distribution plastic failure of the borehole of diameter of 100 mm; (**b**) the distribution plastic failure of the borehole of diameter of 130 mm; (**c**) the distribution plastic failure of the borehole of diameter of 160 mm; (**d**) the distribution plastic failure of the borehole of diameter of 200 mm.
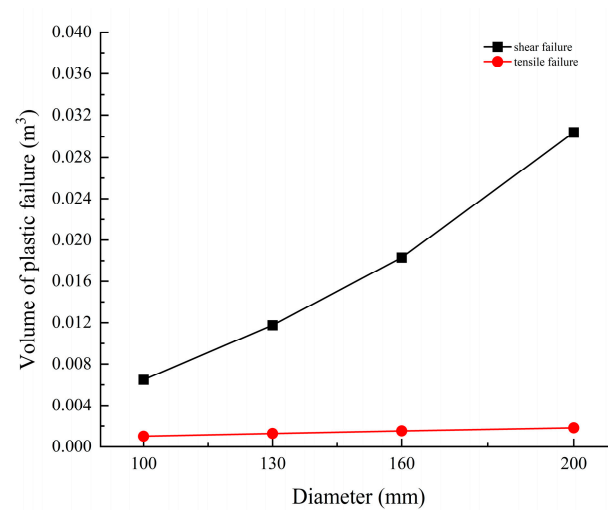

**Figure 11.** The volume of plastic failure zone with different diameters.

In summary, the analysis of the stress state and displacement of the borehole with four diameters of 100 mm, 130 mm, 160 mm, and 200 mm showed that the larger the diameter, the more unstable they are, and the plastic failure volume is directly proportional to the borehole diameter. Therefore, it can be inferred from the comprehensive stress, displacement, and plastic zone that the stability of the borehole decreases as the borehole diameter increases, and the borehole tends to be unstable when the diameters are 160 mm and 200 mm.

2.3. Analysis of Protection Effect of the Hole Protection Pipe

The stability of boreholes is investigated by simulating the application of a borehole protection tube to analyze the protection effect. The modeling process of boreholes is the same as in Section 2.2. The mechanical parameters of the casing are shown in Table 3; the casing is simulated after the borehole is excavated. The model of the casing is shown in Figure 12.
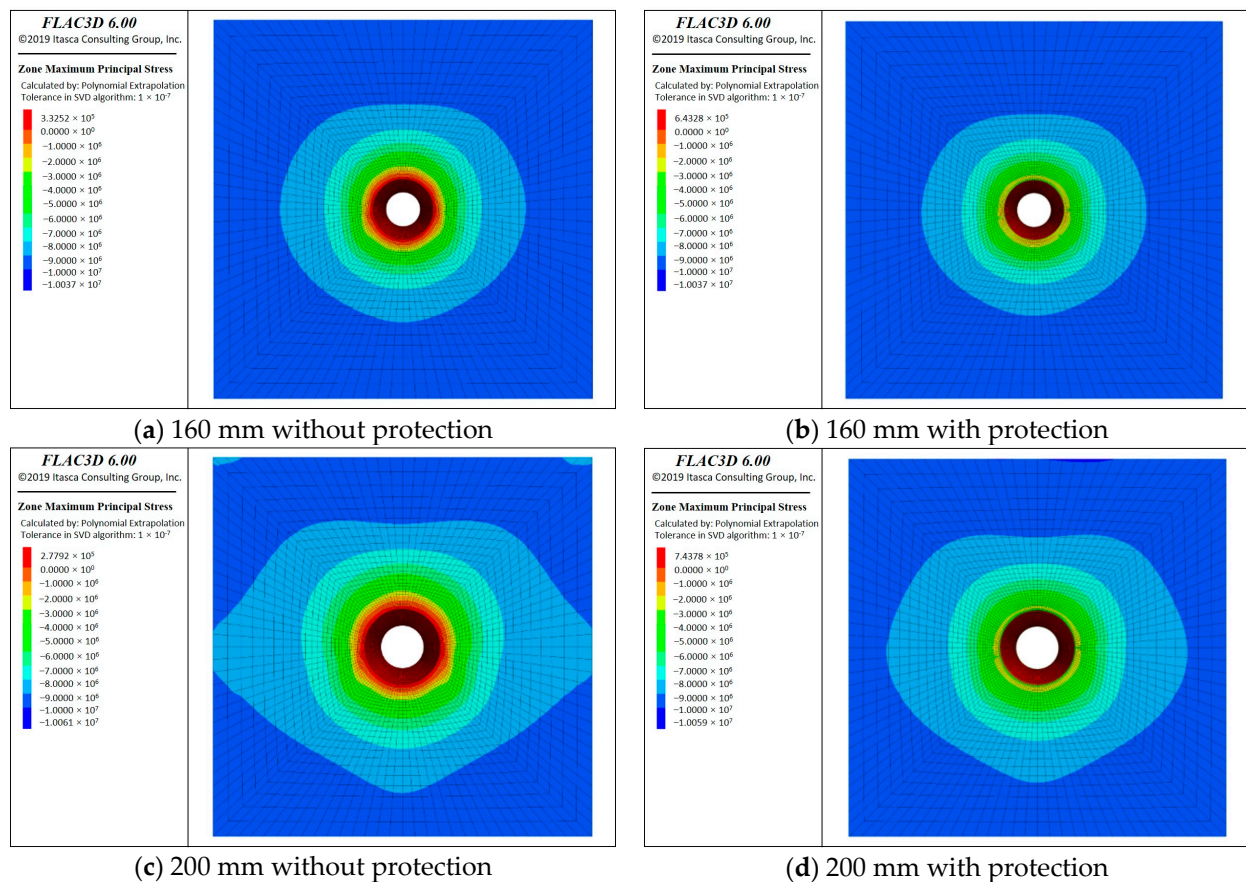
Table 3. Mechanical parameters of the borehole protection pipe.

|	Bulk Modulus/(GPa)	Shear Modulus/(GPa)	Cohesive Strength /(MPa)	Internal Friction/ (°)	Density/(kg/m³)	Tensile Strength/MPa
borehole protection pipe	42.6	33.8	4.8	34	2500	3.9
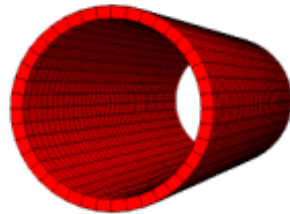
Figure 12. Model of the borehole protection pipe.

### 2.3.1. Analysis of the Stress and Displacement

The maximum principal stress contour of the borehole before and after protection is shown in Figure 13. It can be seen from the contour that the stress concentration at the 160 mm and 200 mm borehole walls is greatly reduced compared to the borehole without the casing. The distribution range of stress concentration is obviously reduced compared to that before protection, especially the stress range before and after borehole protection of 200 mm boreholes changes greatly. This indicates that the borehole protection tube can provide effective support and change the stress state around the borehole wall.

(**a**) 160 mm without protection

(**b**) 160 mm with protection

(**c**) 200 mm without protection

(**d**) 200 mm with protection

Figure 13. Maximum principal stress contours with and without protection.

The displacement monitoring curve of the rock mass around the borehole before and after protection is shown in Figure 14. The displacement changes in the left, upper, and lower protection holes of the 160 mm borehole are 0.2 mm, 3.1 mm, and 2.2 mm respectively. The displacement changes in the left, top, and bottom protection holes of the 200 mm hole are 0.3 mm, 5.4 mm, and 2.7 mm respectively. The results show that the displacement of each monitoring point has obviously changed before and after hole protection, especially the displacement of the upper side of the borehole has the biggest difference. It also shows that the borehole protection pipe can weaken the displacement and deformation caused by borehole excavation, and improve the support and stability of boreholes.
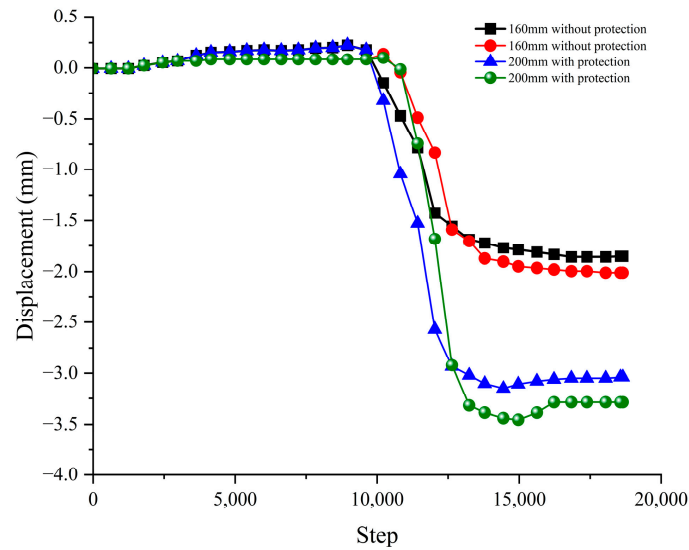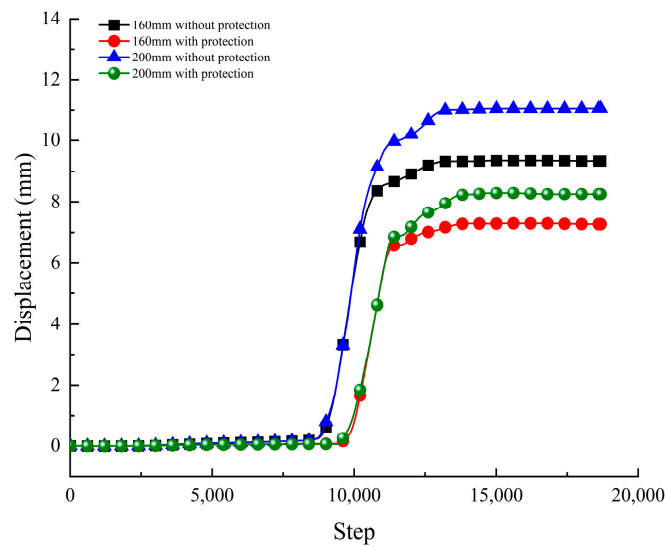

(**a**) Borehole left surrounding rock
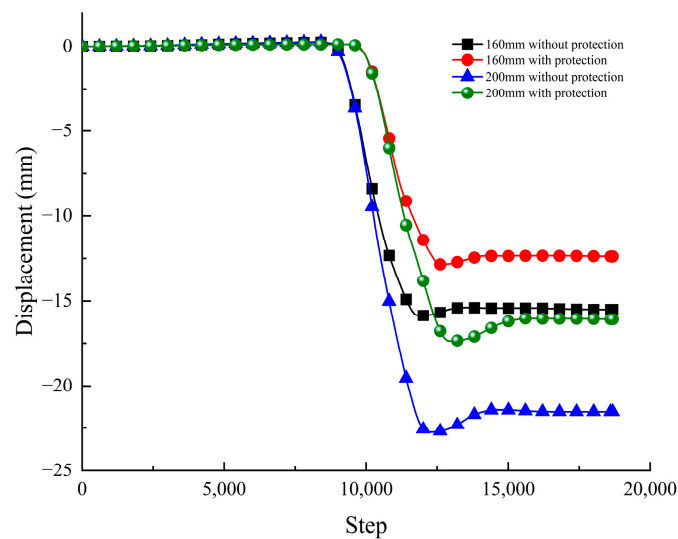
(**b**) Borehole upper surrounding rock

Figure 14. *Cont.*

(**c**) Borehole under a surrounding rock

Figure 14. The variation curve of surrounding rock displacement of the borehole with time.

2.3.2. Analysis of the Plastic Failure

The distribution of plastic failure zones of the boreholes before and after protection is shown in Figure 15. From the plastic distribution diagram, it can be seen that the area of plastic damage of rock mass in 160 mm and 200 mm boreholes are obviously reduced after the application of borehole protection tubes; especially, the area of plastic damage of rock mass in the upper and lower sides of boreholes is the largest. The reduction of the plastic failure zone indicates that the failure instability of the rock mass around the borehole is alleviated, the degree of displacement and deformation is reduced, and the stability of the rock mass around the borehole is strengthened.
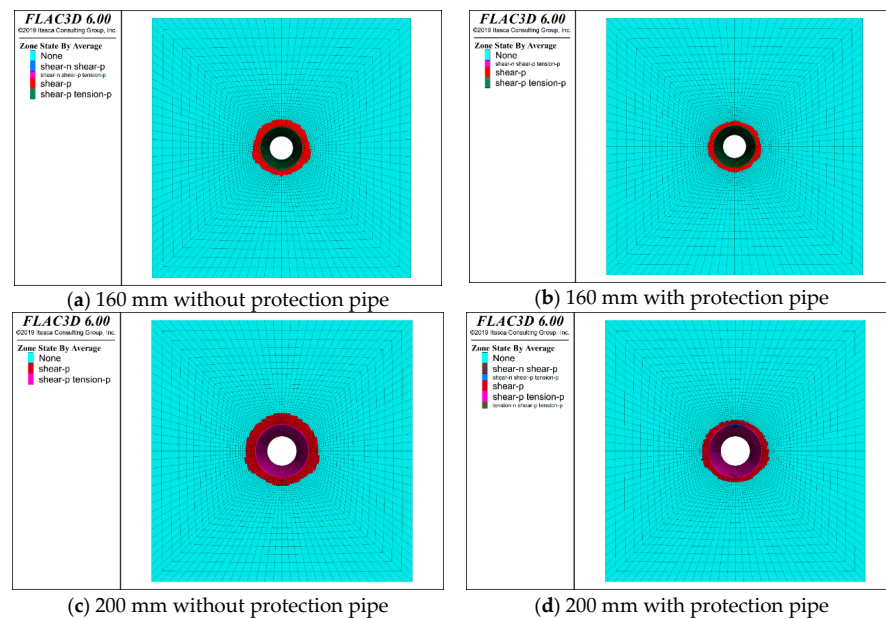

(**a**) 160 mm without protection pipe

(**b**) 160 mm with protection pipe

(**c**) 200 mm without protection pipe

(**d**) 200 mm with protection pipe

Figure 15. Distribution of plastic failure of boreholes with different diameters. (**a**) The distribution plastic failure of the borehole of diameter of 100 mm without protection pipe; (**b**) the distribution plastic failure of the borehole of diameter of 160 mm with protection pipe; (**c**) the distribution plastic failure of the borehole of diameter of 200 mm without protection pipe; (**d**) the distribution plastic failure of the borehole of diameter of 200 mm with protection pipe.

Therefore, it is found that the stress concentration around the borehole is relieved according to the FLAC 3D simulation, the displacement of rock mass around the borehole is reduced, and the plastic damage is reduced, which indicates that the borehole protection tube can provide some protection support. However, for the large boreholes of 160 mm and 200 mm, the strong stress concentration and plastic damage obviously still exist after the protection, and the stability of the borehole needs to be further strengthened.

3. Experimental Study of the Internal Support Borehole Protection Pipe

According to the above analysis of borehole stability, the stability of the directional long borehole on the roof needs to be further improved. The borehole protection pipe is the main measure to change the stability of the borehole, but after using the conventional borehole protection pipe, there is still serious plastic damage and stress concentration phenomenon in directional long boreholes of large diameters. Therefore, the conventional pipe can only improve the stability of the directional long hole in the roof to a certain extent. Therefore, various internal supporting structures are designed to enhance the effect of hole protection, and their effects are studied through compression experiments.

3.1. Experimental Apparatus and Procedures

Three types of borehole protection pipes with internal support structures: "line-shaped", "Y-shaped", and "cross-shaped", are designed as shown in Figure 16. Two common borehole diameters of 100 mm and 160 mm are selected for experimental research.

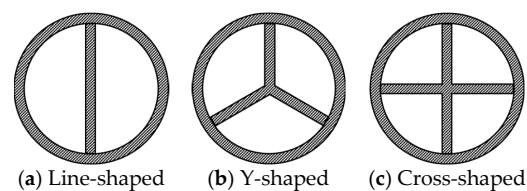(**a**) Line-shaped   (**b**) Y-shaped   (**c**) Cross-shaped

Figure 16. Three internal support structures of the borehole protection pipe.

This experiment is based on the GCTS Rock Mechanics Test System as shown in Figure 17. The system is a hydraulic servo-mechanical system produced by GCTS Company in the United States, which meets the requirements of the ISRM triaxial rock test of the International Society of Rock Mechanics and the American standard ASTM D2664-04. It is mainly used to test the mechanical properties and seepage characteristics of rock, concrete, and coal under complex loading conditions. The test accuracy is high and the performance is stable.
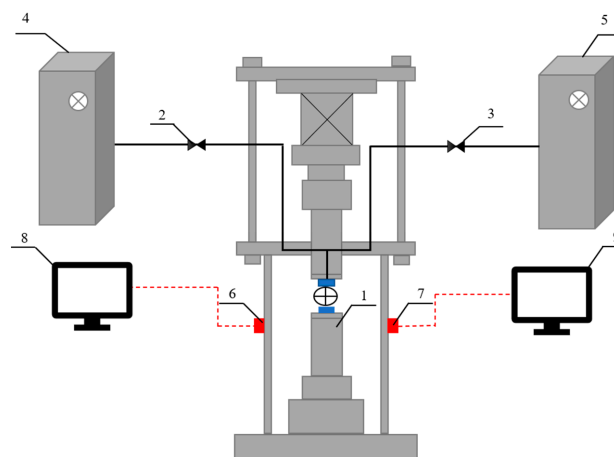

Figure 17. Schematic of the GCTS Rock Mechanics Test System (1 Compression experimental apparatus; 2/3 Controller valve; 4 Control cabinet of confining pressure volume; 5 Control cabinet of pore pressure volume; 6 Radical compressive force sensor; 7 Displacement sensor; 8/9 Storage computer).

The experimental steps of the GCTS rock mechanics test system are as follows:

(1) First, start up the test system and controller, adopt the feedback mode of "displacement control" and debug the system;
(2) Place the sample of the internal support borehole protection tube on the test bench and control the pressure head to move down to fix the sample;
(3) Set the load rate of 10 mm/min uniform speed for the compression test, and then stop after the radial compressive force reaches its peak.

3.2. Test Results

The compression test diagrams of the casing with different internal support structures are shown in Figure 18. All the internal support structures have obvious deformation during the compression process, and the deformation of the internal support structure reduces the deformation of the borehole protection tube so that it can provide good support to the borehole.
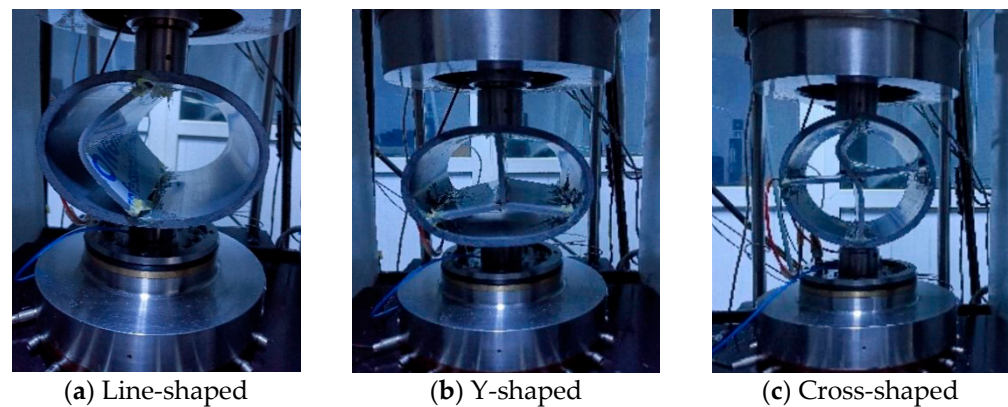

(**a**) Line-shaped   (**b**) Y-shaped   (**c**) Cross-shaped

Figure 18. Three internal support structures of the borehole protection pipe.

The variation of the radial compressive force of the borehole protection tube of different internal support structures of 100 mm and 160 mm is shown in Figures 19 and 20. The peak values of the radial compressive force of 100 mm different support structures are 5.59 kN, 21.03 kN, 11.79 kN, and 29.43 kN respectively. The peak values of the radial compressive force of different 160 mm support structures are 7.29 kN, 18.31 kN, 13.89 kN, and 31.30 kN respectively. The radial compressive force of different internal support structures of the two types of openings are "cross-shaped" > "line-shaped" > "Y-shaped" > Conventional pipe, and the peak compressive force of 160 mm borehole protection pipe is slightly greater than 100 mm.
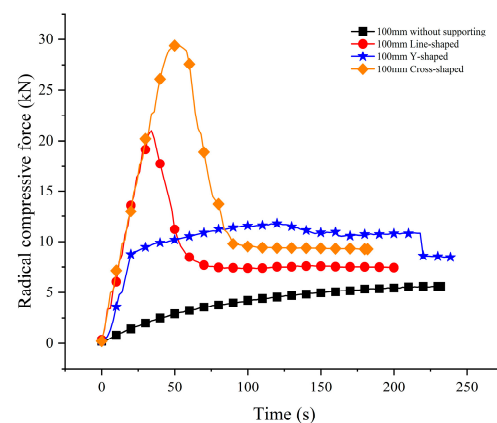

Figure 19. The radial compressive force of 100 mm borehole protection pipe with different internal support structures.
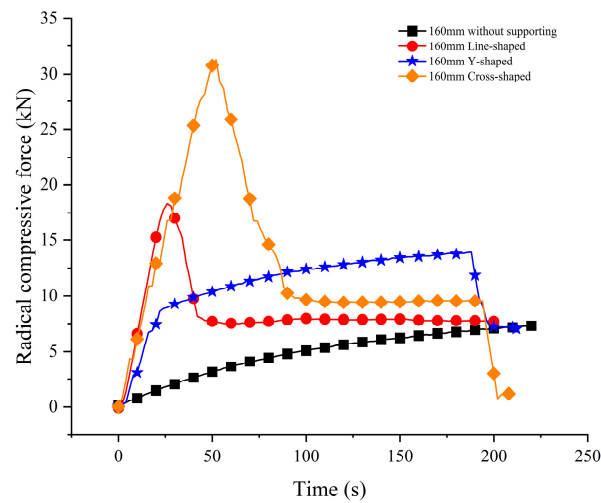
Figure 20. The radial compressive force of 160 mm borehole protection pipe with different internal support structures.

The displacement of different internal support structures in the radial compression test is shown in Figure 21. The displacement trends of 10 mm diameter and 160 mm diameter are basically the same, and the displacement of 160 mm of the same kind of internal support structure is slightly larger than 100 mm; smaller deformation of hole protection tubes are line-shaped and cross-shaped, and the cross-shaped is the smallest.
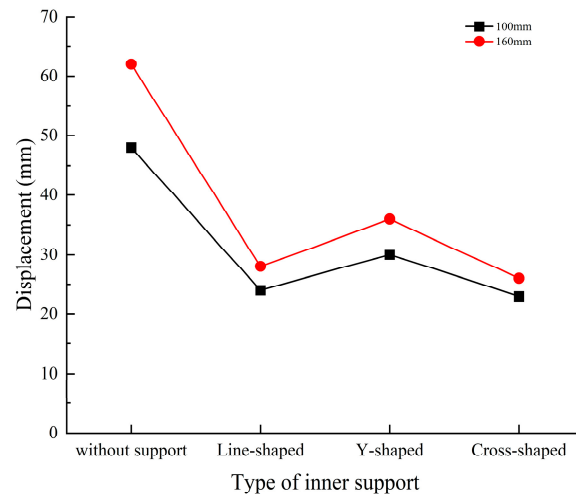

Figure 21. Displacement of borehole protection pipes with different internal support structures at peak compression force.

Therefore, according to the comprehensive analysis of the radial compressive force and deformation of the casing, it can be concluded that all three internal support structures can improve the compression resistance of the casing. Considering that the cross-shaped internal support structure can not only effectively support the vertical compression to resist compression, but also support the pipe wall in the horizontal direction to prevent deformation. Thus, the borehole protection effect of the cross-shaped internal support structure of the borehole protection pipe is the best.

4. Discussion

The directional long borehole on the roof has the characteristics of penetrating more layers and larger borehole diameter. Prior to drilling, the coal seam is in a state of equilibrium under the combined action of overburden pressure, horizontal pressure, and

formation pore pressure. However, the stress balance of the original coal seam is disturbed by the formation of the well, the stress of the coal seam is redistributed, and the pore and fracture structure of the surrounding rock is changed. When the stress in a certain part of the surrounding rock of the borehole exceeds the maximum load that the coal rock can bear, the fractures will spread and penetrate rapidly, and the coal body will be squeezed into the borehole, resulting in instability and collapse of the borehole. From the numerical simulation results, it can be seen that both lithology and borehole diameter significantly influence the stability of roof-directional boreholes. On the one hand, borehole stability is significantly lower in coal and mudstone than in coarse and fine sandstone. Because the mechanical strength of coal and mudstone is lower than that of sandstone, the stress on the rock surrounding the borehole is different, and the radial deformation around the borehole is greater. When the radial deformation reaches the limit, the inner ring coal near the borehole wall fractures and the coal in the fractured area collapses and falls into the borehole. On the other hand, borehole diameter is inversely proportional to borehole stability, and when the borehole diameter exceeds 160 mm, the plastic failure and stress concentration of the borehole are severe and tend to be unstable. Therefore, to avoid instability and collapse of the borehole in soft rock such as coal and mudstone, it is essential to fully consider the rock mass distribution and the selected borehole diameter when designing and constructing directional long boreholes on the roof. Effective hole protection measures must be taken to prevent the failure of critical holes due to the oversized hole diameter.

According to the compression test results, the internal support structure can effectively improve the compression resistance of the conventional borehole protection pipe; especially, the cross-shaped internal support pipe has the best compression resistance which can provide strong support from two directions perpendicular to each other, and the internal support can bear part of the pressure of the borehole protection pipe to keep it in a relatively stable state. The internal supporting structure casing is suitable for roof-directional long holes. Improving the stability of the roof-directional long borehole by the internal support structure borehole protection pipe is beneficial to the efficient gas extraction in the goaf and can promote the popularization and application of the roof-directional long borehole technology. However, the compressive effect of the internal supporting casing cannot be matched with the field effect. Therefore, it is necessary to conduct systematic field experiments in various mines to further investigate borehole protection effects.

5. Conclusions

Borehole construction is the prerequisite for gas extraction in drilling. However, during the drilling construction, factors such as lateral pressure factor, the mechanical strength of rock, confining pressure, and so on are influenced, so that the drilling hole is easily deformed and collapsed, so that the drilling gas extraction performance is poor, and brings hidden hazards to the coal mine safety production. Research on the borehole collapsing law and corresponding borehole protection techniques has great practical significance for preventing borehole distortion and collapsing, increasing borehole stability, and improving gas drainage. Numerical simulations and laboratory experiments have been carried out to investigate the stability of directional long boreholes on the roof, and the main conclusions are as follows:

(1) Under different lithologies, the variation in borehole stress and displacement is significantly greater in coal and mudstone than in coarse and fine sandstone, indicating that borehole stability is strong in fine and coarse sandstone, but weak in coal and mudstone.

(2) With the increase of the borehole diameter, the stress, displacement, and plastic failure volume of the four borehole diameters of 100 mm, 130 mm, 160 mm, and 200 mm increase, that is, the stability of the borehole gradually decreases. The borehole tends to be unstable when the hole diameter is 160 mm and 200 mm.

(3) Stress, displacement, and plastic damage to the rock around the borehole are reduced after the conventional casing is installed. The results show that the conventional

tubing does provide some support to the borehole. However, severe plastic damage and stress concentration still exist when applied to large-diameter borehole protection, so the borehole protection effect is weak.

(4) Compared with the conventional wellbore protection pipe, the peak value of the compressive force of the wellbore protection pipe with line-shaped, Y-shaped, and cross-shaped internal support structures is significantly increased and the displacement is reduced. In particular, the peak value of the compressive force of the cross-shaped internal support structures is four times that of the conventional ones, and the displacement change is half that of the conventional ones. It indicates that the internal support structure can improve the borehole protection effect, and the cross-shaped has the best borehole protection effect.

Due to the limited computing power, the numerical simulation is mainly based on two-dimensional simulation, and many simplifications were made. A closer combination of drilling and mining should be considered for analysis in the future. Moreover, the production cost of the internal support hole protection pipe is higher than that of the common hole protection pipe. Further research should improve and reduce the cost, so as to facilitate the subsequent popularization and application.

Author Contributions: Methodology, Z.W.; conceptualization, X.Y.; formal analysis, X.Y., Z.W., and G.W.; investigation, X.Y. and H.G.; writing—original draft preparation, Z.W. and H.G.; writing—review and editing, X.Y., and H.G.; translation, Z.W.; funding acquisition, X.Y. and G.W. All authors have read and agreed to the published version of the manuscript.

Data Availability Statement: The data that support the findings of this study are available from the corresponding author upon reasonable request.

Conflicts of Interest: The authors declare that they have no known competing financial interests or personal relationships that could have appeared to influence the work reported in this paper.

References

1. Liu, Z.; Cheng, Y.; Jiang, J.; Li, W.; Jin, K. Interactions between coal seam gas drainage boreholes and the impact of such on borehole patterns. *J. Nat. Gas Sci. Eng.* **2017**, *38*, 597–607. [CrossRef]
2. Cheng, Z.; Pan, H.; Zou, Q.; Li, Z.; Chen, L.; Cao, J.; Zhang, K.; Cui, Y. Gas flow characteristics and optimization of gas drainage borehole layout in protective coal seam mining: A case study from the Shaqu coal mine, Shanxi province, China. *Nat. Resour. Res.* **2020**, *30*, 1481–1493. [CrossRef]
3. Lin, H.; Huang, M.; Li, S.; Zhang, C.; Cheng, L. Numerical simulation of influence of Langmuir adsorption constant on gas drainage radius of borehole in coal seam. *Int. J. Min. Sci. Technol.* **2016**, *26*, 377–382. [CrossRef]
4. Wei, P.; Huang, C.; Li, X.; Peng, S.; Lu, Y. Numerical simulation of boreholes for gas extraction and effective range of gas extraction in soft coal seams. *Energy Sci. Eng.* **2019**, *7*, 1632–1648. [CrossRef]
5. Zhang, X.; Gao, J.; Jia, G.; Zhang, J. Study on the influence mechanism of air leakage on gas extraction in extraction boreholes. *Energy Explor. Exploit.* **2022**, *40*, 1344–1359. [CrossRef]
6. Wang, G.; Fan, C.; Xu, H.; Liu, X.; Wang, R. Determination of long horizontal borehole height on the roofs and its application to gas drainage. *Energies* **2018**, *11*, 2647. [CrossRef]
7. Li, H.; Liu, Y.; Wang, W.; Liu, M.; Ma, J.; Guo, X.; Guo, H. The integrated drainage technique of directional high-level borehole of super large diameter on the roof replacing roof extraction roadway: A case study of the underground Zhaozhuang Coal Mine. *Energy Rep.* **2020**, *6*, 2651–2666. [CrossRef]
8. Wang, J. Research and application of pressure relief gas drainage technology by long borehole along large diameter from roof fracture zone. *IOP Conf. Ser. Earth Environ. Sci.* **2019**, *358*, 032011. [CrossRef]
9. Duan, H.; Wang, Y.; Xiao, Q.; Wang, J.; Peng, D. Gas extraction technology and application of near horizontal high directional borehole. *Energy Rep.* **2022**, *8*, 1326–1333. [CrossRef]
10. Li, T.; Wu, B.; Lei, B. Study on the optimization of a gas drainage borehole drainage horizon based on the evolution characteristics of mining fracture. *Energies* **2019**, *12*, 4499. [CrossRef]

11. Yao, X.; Cheng, G.; Shi, B. Analysis on gas extraction borehole instability and control method of pore-forming in deep surrounding-rock with weak structure. *J. China Coal Soc.* **2010**, *35*, 2073–2081. [CrossRef]

12. Karatela, E.; Taheri, A. Three-dimensional hydro-mechanical model of borehole in fractured rock mass using discrete element method. *J. Nat. Gas Sci. Eng.* **2018**, *53*, 263–275. [CrossRef]

13. Yurum, Y.; Bozkurt, D.; Yalcin, M.N. Change of the structure of coals from the Kozlu K20 G borehole of Zonguldak basin with burial depth 2. macromolecular structure. *Energy Sources* **2001**, *23*, 521–527. [CrossRef]

14. Zhang, N.; Xue, F.; Zhang, N.; Feng, X. Patterns and security technologies for co-extraction of coal and gas in deep mines without entry pillars. *Int. J. Coal Sci. Technol.* **2015**, *2*, 66–75. [CrossRef]

15. Yang, C.; Liu, J. Petroleum rock mechanics: An area worthy of focus in geo-energy research. *Adv. Geo-Energy Res.* **2021**, *5*, 351–352. [CrossRef]

16. Ding, L.; Wang, Z.; Liu, B.; Lv, J.; Wang, Y. Borehole stability analysis: A new model considering the effects of anisotropic permeability in bedding formation based on poroelastic theory. *J. Nat. Gas Sci. Eng.* **2019**, *69*, 102932. [CrossRef]

17. Zhao, H.; Li, J.; Liu, Y.; Wang, Y.; Wang, T.; Cheng, H. Experimental and measured research on three-dimensional deformation law of gas drainage borehole in coal seam. *Int. J. Min. Sci. Technol.* **2020**, *30*, 397–403. [CrossRef]

18. Katanov, Y.; Vaganov, Y.; Cheymetov, M. Neural simulation-based analysis of the well wall stability while productive seam penetrating. *Min. Miner. Depos.* **2021**, *15*, 91–98. [CrossRef]

19. Ma, Y.; Xu, Y. Research into technology for precision directional drilling of gas-drainage boreholes. *Min. Miner. Depos.* **2022**, *16*, 27–32. [CrossRef]

20. Dychkovskyi, R.O.; Lozynskyi, V.H.; Saik, P.B.; Petlovanyi, M.V.; Malanchuk, Y.Z.; Malanchuk, Z.R. Modeling of the disjunctive geological fault influence on the exploitation wells stability during underground coal gasification. *Arch. Civ. Mech. Eng.* **2018**, *18*, 1183–1197. [CrossRef]

21. Petlovanyi, M.; Lozynskyi, V.; Saik, P.; Sai, K. Predicting the producing well stability in the place of its curving at the underground coal seams gasification. *E3S Web Conf.* **2019**, *123*, 01019. [CrossRef]

22. Zhang, X.; Wang, W.; Yang, M. Study on deformation and destabilization characteristics and modes of drainage borehole. *Energy Sources* **2020**, *42*, 2448–2459. [CrossRef]

23. Qu, P.; Shen, R.; Fu, L.; Wang, Z. Time delay effect due to pore pressure changes and existence of cleats on borehole stability in coal seam. *Int. J. Coal Geol.* **2011**, *85*, 212–218. [CrossRef]

24. Niu, Y.; Song, X.; Li, Z.; Wang, E.; Liu, Q.; Zhang, X.; Cai, G.; Zhang, Q. Experimental study and field verification of stability monitoring of gas drainage borehole in mining coal seam. *J. Pet. Sci. Eng.* **2020**, *189*, 106985. [CrossRef]

25. Niu, Y.; Zhang, X.; Wang, E.; Li, Z.; Cheng, Z.; Duan, X.; Li, H.; Wei, Y.; Qian, J.; Cai, G.; et al. A new method of monitoring the stability of boreholes for methane drainage from coal seams. *Measurement* **2020**, *154*, 107521. [CrossRef]

26. Zhang, Q.; Wang, E.; Li, Z.; Wang, H.; Xue, Z. Control of directional long borehole on gas drainage and optimal design: Case study. *J. Nat. Gas Sci. Eng.* **2022**, *107*, 104766. [CrossRef]

27. Xu, B.L.; Liu, S.Y.; Li, H.S. Drill string's axial force transfer law in slide directional drilling in underground coal mine. *Tunn. Undergr. Space Technol.* **2022**, *130*, 104701. [CrossRef]

28. Liu, J.; Wu, Z.; Lu, P.; Liu, Z.; Su, M. Study on Effective Extraction Radius of Directional Long Borehole and Analysis of the Influence Mechanism. *ACS Omega* **2023**, *8*, 2344–2356. [CrossRef]

29. Yuan, S.; Han, G. Combined Drilling Methods to Install Grout Curtains in a Deep Underground Mine: A Case Study in Southwest China. *Mine Water Environ.* **2020**, *39*, 902–909. [CrossRef]

30. Yuan, S.; Sun, B.; Han, G.; Duan, W.; Wang, Z. Application and Prospect of Curtain Grouting Technology in Mine Water Safety Management in China: A Review. *Water* **2022**, *14*, 4093. [CrossRef]

31. Wang, H.; Kou, Z.; Guo, J.; Chen, Z. A semi-analytical model for the transient pressure behaviors of a multiple fractured well in a coal seam gas reservoir. *J. Pet. Sci. Eng.* **2020**, *198*, 108159. [CrossRef]

32. Wang, S.; Wang, S. Longwall mining automation horizon control: Coal seam gradient identification using piecewise linear fitting. *Int. J. Min. Sci. Technol.* **2022**, *32*, 821–829. [CrossRef]

33. Xue, F.; Zhang, N.; Feng, X.; Zheng, X.; Kan, J. Strengthening borehole configuration from the retaining roadway for greenhouse gas reduction: A case study. *PLoS ONE* **2015**, *10*, e0115874. [CrossRef] [PubMed]

34. Zhai, C.; Xu, Y.; Xiang, X.; Yu, X.; Zou, Q.; Zhong, C. A novel active prevention technology for borehole instability under the influence of mining activities. *J. Nat. Gas Sci. Eng.* **2015**, *27*, 1585–1596. [CrossRef]

35. Di, C.; Li, Q.; Sun, C.; Ni, G.H.; Yang, W. Analysis on borehole instability and control method of poreforming of hydraulic fracturing in soft coal seam. *J. China Coal Soc.* **2012**, *37*, 1431–1436. [CrossRef]

36. Qi, Q.; Jia, X.; Zhou, X.; Zhao, Y. Instability-negative pressure loss model of gas drainage borehole and prevention technique: A case study. *PLoS ONE* **2020**, *15*, e0242719. [CrossRef]

37. Li, H.; Wang, W.; Liu, Y.; Ma, J.; Gao, H. An integrated borehole, protection and sealing technology for improving the gas drainage effect in soft coal seams. *Energy Rep.* **2020**, *6*, 2030–2043. [CrossRef]

38. Xu, H.; Fang, Z.; Sang, S.; Liu, H.; Ding, H.; Dou, X.; Liu, Q. Analysis of the shear failure of surface methane capture boreholes for improving the drainage period efficiency: A lithological perspective. *Energy Explor. Exploit.* **2019**, *38*, 92–100. [CrossRef]

39. Meier, T.; Rybacki, E.; Reinicke, A.; Dresen, G. Influence of borehole diameter on the formation of borehole breakouts in black shale. *Int. J. Rock Mech. Min. Sci.* **2013**, *62*, 74–85. [CrossRef]

40. Ji, Q. Research and application of auger-air borehole and sieve pipe borehole protection in soft outburst-prone coal seams. *Procedia Eng.* **2014**, *73*, 283–288. [CrossRef]